Comparison of plasmon surface waves on shallow and deep metallic 1D and 2D gratings

E. Popov, Nicolas Bonod, Stefan Enoch

Comparison of plasmon surface waves on shallow and deep metallic 1D and 2D gratings

Evgeny Popov, Nicolas Bonod, and Stefan Enoch

Institut Fresnel, Unité mixte de recherche de CNRS 6133, Université de Provence, case 161, ave. Escadrille Normandie-Niemen, 13397 Marseille, Cedex 20,
e.popov@fresnel.fr

Abstract: The propagation of a plasmon surface wave in deep metallic lamellar gratings is shown to be characterized by absorption losses smaller than on a flat metallic-dielectric interface. This feature is due to the formation of a resonance of the electric field inside the groove. Similar to the plasmon surface wave in shallow gratings, this kind of plasmon can lead to total absorption of incident light and to a significant enhancement of the local field density in the vicinity of the grating surface, contrary to the other type of grating anomaly linked with a cavity resonance.

OCIS codes: (240.6680) Surface plasmons; (050.1950) Diffraction gratings

References and links

1. R. W. Wood, "On a remarkable case of uneven distribution of light in a diffraction grating spectrum," Phylos. Mag. **4**, 396-402 (1902).
2. U. Fano, "The theory of anomalous diffraction gratings and of quasi-stationary waves on metallic surfaces (Sommerfeld's waves)," J. Opt. Soc. Am. **31**, 213-222 (1941).
3. A. Hessel and A. A. Oliner, "A new theory of Wood's anomalies on optical gratings," Appl. Opt. **4**, 1275-1297 (1965).
4. D. A. Weitz, T. J. Gramila, A. Z. Genack, and J. I. Gersten, "Anomalous low-frequency Raman scattering from rough metal surfaces and the origin of the surface-enhanced Raman scattering," Phys. Rev. Lett. **45**, 355-358 (1980).
5. T. Ebbesen, H. Lezec, H. Ghaemis, T. Thio, and P. Wolff, "Extraordinary optical transmission through sub-wavelength hole arrays," Nature **391**, 667 – 669 (1998).
6. M. J. Levene, J. Korlach, S. W. Turner, M. Foquet, H. G. Craighead, and W. W. Webb**, "**Zero-Mode Waveguides for Single-Molecule Analysis at High Concentrations," Science **299**, 682-686 (2003).
7. J. B. Pendry, L. Martin-Moreno, F. J. Garcia-Vidal, "Mimicking Surface Plamsons with Structured Surfaces," Science **305**, 847-848 (2004)
8. P. Hibbins, M. J. Lockyear, I. R. Hooper, J. R. Sambles,"Waveguide arrays as metamaterials: transmission below cut-off," Phys. Rev. Lett. **96**, 073904 (2006)
9. E. Popov, L. Tsonev, and D. Maystre, "Losses of plasmon surface wave on metallic grating," J. Mod. Opt. **37**, 379-387 (1990).
10. T. López-Rios, D. Mendoza, F. J. Garcia-Vidal, J. Sánchez-Dehesa, and B. Pannetier, "Surface shape resonances in lamellar metallic gratings," Phys. Rev. Lett. **81**, 665-668 (1998).
11. F. J. Garcia-Vidal, J. Sánchez-Dehesa, A. Dechelette, E. Bustarret, T. López-Rios, T. Fournier, and B. Pannetier, "Localized surface plasmons in lamellar metallic gratings," J. Lightwave Technol. **17**, 2191-2195 (1999).
12. W.-C. Tan, T. W. Preist, J. R. Sambles, and N. P. Wanstall, "Flat surface-plasmon-polariton bands and resonant optical absorption on short-pitch metal gratings," Phys. Rev. B **59**, 12661 (1999)
13. R. Hooper, J. R. Sambles, "Surface plasmon polaritons on narrow-ridged short-pitch metal gratings," Phys. Rev. B **66**, 205408 (2002)
14. H. J. Lezec and T. Thio, "Diffracted evanescent wave model for enhanced and suppressed optical transmission through subwavelength hole array," Opt. Express **12**, 3629-3651 (2004)
15. M. Nevière and E. Popov, *Light Propagation in Periodic Media: Diffraction Theory and Design*, (Marcel Dekker, New York, 2003).
16. Lord Rayleigh O. M., "Note on the remarkable case of diffraction spectra described by prof. Wood," Phil. Mag. **14**, 60-65 (1907).

17. See, for example, the review chapter by D. Maystre, "General study of grating anomalies from electromagnetic surface modes," in *Electromagnetic Surface Modes*, A. D. Boardman, ed. (John Wiley, 1982), ch.17.
18. R. Reinisch, E. Popov, and M. Nevière, "Second harmonic generation induced optical bistability in prism or grating couplers," Opt. Lett. **20**, 854-856 (1995)
19. B. S. Thornton, "Limit of the moth's eye principle and other impedance-matching corrugations for solar-absorber design," J. Opt. Soc. Am. **65**, 267-270 (1975).
20. R. C. McPhedran, G. H. Derrick, and L. C. Botten, "Theory of crossed gratings," in *Electromagnetic Theory of Gratings*, R. Petit, ed. (Springer, Berlin, 1980)
21. E. Popov, L. Tsonev, and D. Maystre, "Lamellar diffraction grating anomalies," Appl. Opt. **33**, 5214-5219 (1994).
22. E. Popov, L. Tsonev, and D. Maystre, "Gratings-General properties of the Littrow mounting and energy flow distribution," J. Mod. Opt. **37**, 367-377 (1990)
23. See, for example, M. Neviere, "The homogeneous problem," in *Electromagnetic theory of gratings*, R. Petit ed. (Springer-Verlag, 1980), ch.5.
24. A.-L. Baudrion, J.-C. Weber, A. Dereux, G. Lecamp, P. Lalanne, S. I. Bozhevolnyi, "Influence of the filling factor on the spectral properties of plasmonic crystals," Phys. Rev. B **74**, 125406 (2006)
25. E. Popov, M. Nevière, S. Enoch, R. Reinish, "Theory of light transmission through subwavelength periodic hole arrays," Phys. Rev. B **62**, 16100-16108 (2000).
26. A. H. van Nieuwstadt, M. Sandtke, R. H. Harmsen, F. B. Segerink, J. C. Prangsma, S. Enoch, and L. Kuipers, "Strong modification of the nonlinear optical susceptibility of metallic subwavelength hole arrays," Phys. Rev. Lett. **97**, 146102 (2006).
27. J. D. Jackson, *Classical Electrodynamics* (Wiley, 1998), sec. 8.5.

1. Introduction

Plasmon surface waves that are supported by a metal-dielectric interface are known to play a major role in many domains of optics, spectroscopy, chemistry, and biophysics. If the history has started with Wood's discovery of grating anomalies [1] finding its links with the plasmon surface waves in the works of Fano [2] and Hessel and Oliner [3], their importance in periodic structures has not been rerouted by the interest devoted to SERS [4] in the 1980s'. On the contrary, during the entire 20^{th} century surface waves anomalies have attracted attention of grating manufacturers and theoreticians in order to avoid or to use them in different applications. The interest was revived dramatically in 1998 by work of Ebbesen [5], followed by tens of thousands of published works devoted to enhanced transmission through periodically pierced metallic layers. Surface plasmon excitation allows for increasing of electromagnetic field density even in single apertures, which starts to serve for single-molecule detection [6] in chemistry and biology. All this has recently led to creating a domain of optics called 'plasmonics,' which resembles quite strangely the boom of Integrated optics more than 30 years ago. However, despite the similarities between these two domains of modern optics, there is a quite important difference between them, due to the fact that contrary to the integrated optics, the plasmonic deals with metals that have much more important absorption losses than the dielectric waveguides. The only domain where these losses become negligible is the microwave region, but unfortunately surface plasmons are nor supported there. However, it has been recently shown that surface plasmon-like wave can propagate on the surface of infinitely conducting gratings [7-8]. Homogenization of the structured layer shows that suitably corrugated metal present surface wave with a relation dispersion similar to those of surface plasmon.

The aim of this work is to analyze the behavior of another type of surface plasmons, which exist on deep-groove gratings and are characterized by smaller absorption losses. The physical reason for these lower losses is the appearance of a standing wave inside the grooves formed by the fundamental TEM waveguide mode. This phenomenon has already been studied theoretically in sinusoidal gratings [9] but progress in nanotechnologies triggered a new interest in short period gratings. The problem of plasmon surface waves (PSW) in lamellar metallic gratings and hole arrays has been the subject of extensive theoretical, numerical, and experimental studies during the last decade. In particular, there has been demonstrated theoretically and experimentally that deep corrugations can support new kind of plasmon

modes created by the coupling between the plasmon surface wave and the groove cavity resonances [10-11]. It has also been shown that surface plasmons in deep and narrow Gaussian grooves exhibit very flat dispersion curves [12]. Totally different situation is observed when considering deep and narrow Gaussian ridges [13].

However, there is still a discussion about the physical nature of PSW and the role played by the groove resonances. Some authors have proposed the existence of another mechanism distinct from the PSW denoted as a composite diffracted evanescent wave [14]. Our comparative study of the PSW in shallow and deep grooves enable to clarify their common nature including the energy flow distribution and local field enhancement. Contrary to several previous studies [10-11], the energy flow distribution above the groove top presents a non-localized (propagating) character, for deep grooves as well as for shallow gratings. The other new feature is the possibility to obtain smaller decay constant of the surface wave in deep gratings, a fact that could be used in plasmonic devices.

The study is made using the differential method for modeling light diffraction by periodic structures [15]. The analysis of the field maps and the Poynting vector direction shows the great similarity between the first (for shallow grooves) and the second (for deep grooves) kind of plasmon surface waves and the differences between them and the cavity resonances.

2. Light absorption by lamellar metallic gratings and plasmon surface wave excitation

As already discussed, the influence of plasmon excitation on the efficiency of metallic gratings has been at first observed experimentally by Wood [1], the effect has attracted the attention of Lord Rayleigh [16], leaving the name of Rayleigh anomalies to the cut-off effects due to the disappearance of a given diffracted order when the angle of incidence or/and the wavelength are varied. In particular, shallow gratings were demonstrated to totally absorb the incident light under special conditions [17], an analogue of the famous Brewster effect for plane dielectric interfaces.

A plane aluminum-air interface can support plasmon surface wave and in the red (wavelength λ = 0.6328 μm, aluminum refractive index equal to n_{AL} = 1.378 + i 7.616) its effective index is equal to $\alpha_p = k_x/k_0$ = 1.0079 + i 0.003, where k_p is the surface wave propagation constant and $k_0=2\pi/\lambda$ is the free-space wavenumber. In what follows, all dimensions will be expressed in microns and the dispersion of aluminum is not taken into account, in order to simplify the understanding, because otherwise the spectral behavior will be complicated by the refractive index dispersion.

As is well-known, a periodic corrugation can lead to a coupling between the incident plane wave and the surface wave, provided a necessary phase condition coming from the grating equation is satisfied:

$$\alpha = \alpha_p + m\frac{\lambda}{d} \qquad (1)$$

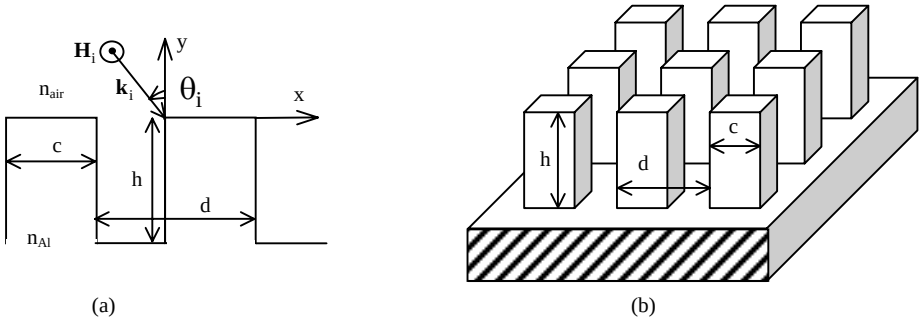

Fig.1. Schematic representation of lamellar grating with notations. One-dimensional (a) and 2-dimensional (b) geometry.

where $\alpha = \sin\theta_i$ is linked to the angle of incidence, m is integer, and d is the corrugation period (see Fig.1(a)). On the other hand, this coupling is reciprocal, i.e., the surface wave can be radiated into the cladding in the directions given by eq.(1). This outcoupling leads to radiation losses which are expressed as an increase of the imaginary part of the mode propagation constant. In addition, as the surface corrugation deepens, the absorption in the substrate increase, in general, thus contributing to the increase of the plasmon decay constant.

The competition between the transfer of energy to the surface wave and its radiation in the propagating orders (and, more important, change in the phase difference between these two processes when the corrugation depth increases) leads to the existence of an optimal groove depth for maximal absorption. It is generally at almost the same conditions when the intensity of the surface wave is maximal and so is the local field density in the close vicinity of the corrugated interface. As already mentioned, this effect has found numerous application in SERS, nonlinear optical effects [18], solar absorption cells based on grating structures [19-20], etc.

It is possible to obtain an almost total absorption (and thus maximum local field enhancement) only when the structure supports small number of diffraction orders, otherwise the competition between them spoils the absorption. In particular, the best configuration requires that only the specular order propagates, although in some case (as demonstrated later) it is possible to achieve almost total absorption of the incident light with two propagating orders. As it is well-known, for aluminum in the red, the optimal plasmon excitation appears at about 10% modulation depth h (compared to the groove period d). This can be observed in Fig. 2, which presents the total diffracted efficiency (the sum of the zeroth and the -1^{st} order, when existing) as a function of the lamella width c and groove depth h.

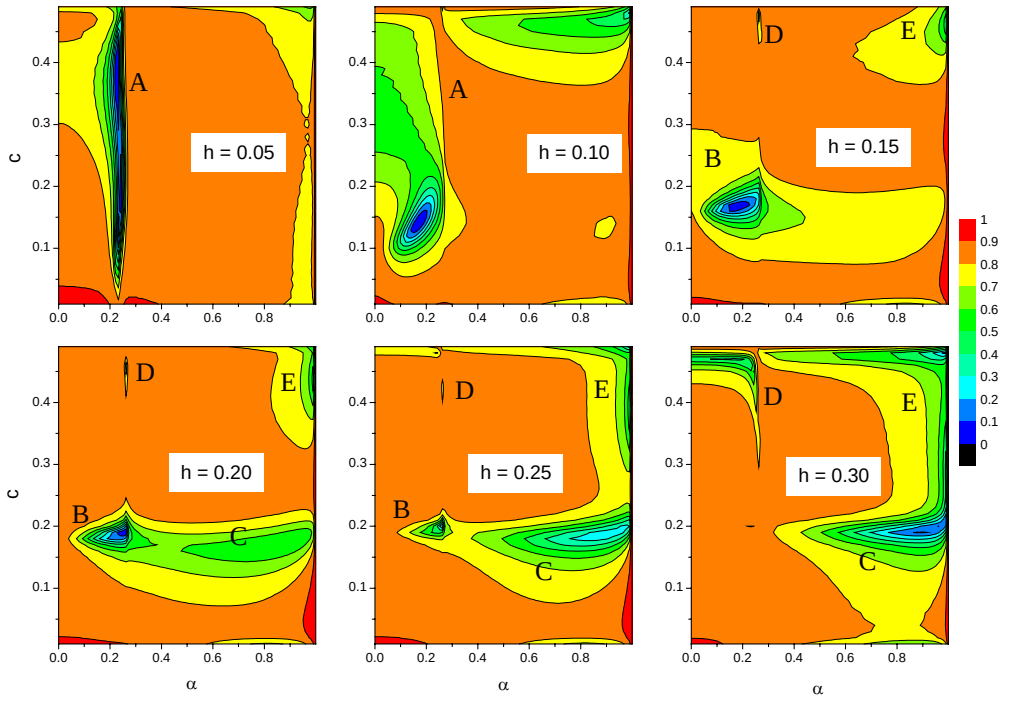

Fig.2. Total reflected energy as a function of the sinus α of the incident angle and the lamella width c (in μm) for several groove depth values h (labelled in nm). Period d = 0.5 μm, wavelength λ = 0.6328 μm.

For h = 0.05 and independently of the lamella width c, one can observe a sharp drop in the total reflectivity very close to the -1^{st} order angle of appearance (cut-off), corresponding to $\alpha = 0.2656$, region labeled as A in Fig. 2 .When increasing the corrugation depth, the absorption due to the plasmon surface wave excitation is reduced, as already discussed and as observed in the rest of Fig. 2 in the region lying close to the line $\alpha = 0.2656$ (region labeled with A). In order to study the behavior of the mode, we have calculated the normalized propagation constant α_p of the plasmon surface mode, which represents a complex pole of the determinant of the scattering matrix S, $\det[S^{-1}(\alpha_p)]=0$, and the results are given in Fig.3. The decrease of absorption can be understood taking into account the fact that the increase of the groove depth leads to an increase of the imaginary part of the mode propagation constant (radiation and absorption losses included), as observed in Fig.3a, an increase which depends on the groove filling factor. In particular, for c = 0.18 the increase is less pronounced, which leads to a larger in h extension of the anomaly (see the region labeled as B in Fig. 2). In addition to the increase of the imaginary part, one finds an augmentation of the real part as well (Fig.3b), which moves the position of the anomaly from the -1^{st} order cut-off toward the normal incidence, as confirmed in Fig. 2 for h = 0.15 and 0.20, but with a diminishing absorption.

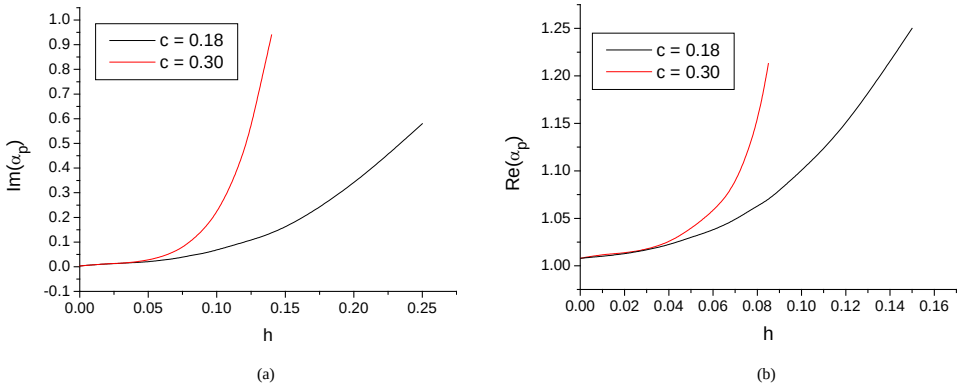

Fig.3. Variation of the imaginary (a) and the real (b) part of the mode effective index as a function of the groove depth for two filling factors (i.e. lamella width c).

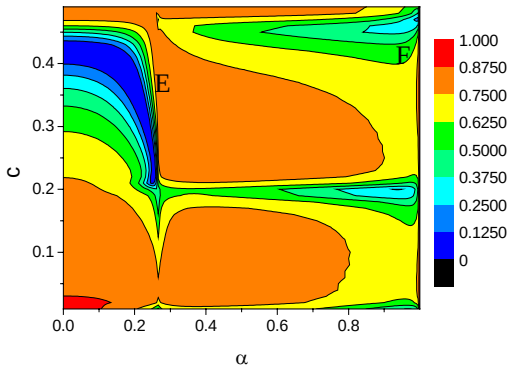

Fig.4. The same as in Fig. 2 but for h = 0.35 μm.

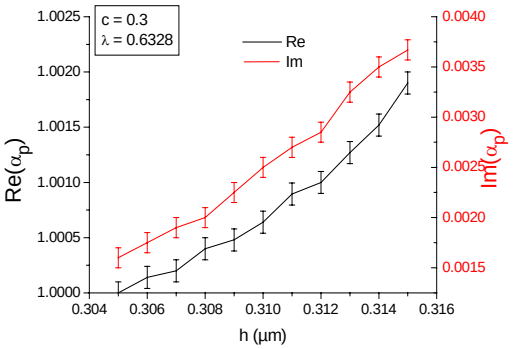

Fig.5. The mode effective index (normalized propagation constant) as a function of the groove depth for the secondary plasmon mode, existing for deeper grooves

Despite the fact that these results and their consequence are well-known [17] we find it necessary to repeat them in view of the following considerations. At first, when the groove depth is sufficiently large, other anomalies appear. These are the Fabry-Perot resonances of the fundamental TEM mode (that can always propagate without a cut-off inside even a very narrow slit), which is responsible for the anomalies appearing close to the value of c approaching 0.5 (narrow grooves). The second feature (labeled C) found close to c = 0.18 for $\alpha > 0.4$ is due to cavity resonances, appearing when a multiple entities (approximately, for non-perfectly conducting materials) of half-wavelengths can fit inside the groove depth and width. They can lead to high absorption values, but their role in the increase of local field density is quite limited, leading to an increase of 2-4 times [21] when compared to the tens-fold increase due to the surface wave excitation. The angular tolerances of excitation of these cavity resonances are quite large, as observed in particular in Fig. 2 for h = 20, 25, and 30 nm, where the position of the anomaly (label C) is practically independent of the angle of incidence (anyway, staying in the limits where both the zeroth and –1st diffraction orders propagate, i.e. $\alpha > 0.2656$).

Our main target is the small feature (label D) that appears for $h \geq 0.15$ in the region $c \geq 0.4$ close to the –1st order cut-off and which extends to just below c = 0.3 for h = 0.3. This feature is also visible in the region (labeled as E) close to $\alpha \approx 1$ (in fact, due to the symmetry, close to $\alpha \approx \pm 1$), which corresponds to an interaction between $\alpha \approx 0.2656$ and $\alpha \approx -1$ through the order with m = 1 in eq.(1), and we shall return to this fact later. Fig. 4 for h = 0.35 μm shows the extension of this anomaly to a quite large interval of filling factors, pointing out to the generality of the phenomenon. Its importance can be better understood when comparing the imaginary parts of the normalized propagation constants, Fig.3(a) for the first kind of plasmon surface wave (supported by shallow corrugations), and Fig. 5 for the second kind plasmon (supported by deep grooves). As can be observed in Fig. 5, the second kind plasmon surface wave (PSW) is characterized by a decay constant weaker than that for a flat interface. This second kind of PSW appears for h = 0.305 μm and, as can be observed in Fig. 5, its decaying constant has an imaginary part of 0.0016, almost twice weaker than that for a flat interface, i.e. the propagation length is twice larger. This leads to a narrower angular width of anomaly in reflection due to the excitation of the second kind of PSW, Fig. 6.

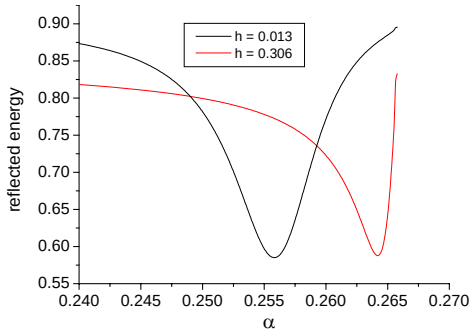

Fig.6. Reflection by the lamellar grating as a function of the angle of incidence (in a) when either the first (h small and equal to 0.013 μm) or the second (h = 0.306 μm) type plasmon surface wave is excited . Lamella width c = 0.3 μm.

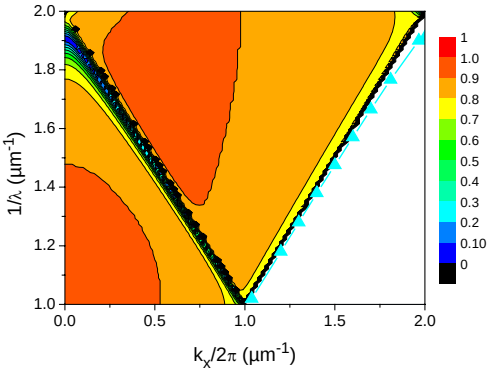

Fig.7. Dispersion curves (cyan lines with the triangle symbols to the right) together with the total reflected intensity (to the left) corresponding to the plasmon surface wave excitation for shallow grooves, c = 0.3 μm, h = 0.036 μm.

There are two natural questions that arise with respect to the above results and the following considerations. First, whether the phenomenon really corresponds to a surface wave, a localized wave [11], or to a cavity resonance. Second, whether it leads to an important enhancement of the field density. In order to answer these questions, it is necessary to look in the near-field map and energy flow distribution, together with the analysis of the dispersion curves.

3. Mode dispersion curves (ω-k) and near-field maps

The dispersion (ω-k) curves of a PSW for shallow corrugations is quite similar to the dispersion curve without corrugation, shown in Fig. 7. Neglecting the spectral dispersion of the aluminum refractive index, the dispersion curve is a line parallel to the straight ω/c. Due to the coupling at the boundaries of the Brillouin zone, the straight line is deformed when the interaction between the PSW propagating in opposite directions becomes stronger. In Fig.8 we can observe that the so-assumed as-up-to-now second kind PSW has a propagation constant (shown in cyan) which follows quite well a line adjacent to the light cone ω/c, but staying outside it (in white region in Fig.8), a behavior similar to the usual PSW at shallow grooves in Fig. 7. Increasing ω/c increases the interaction between the counter-propagating waves and so the deviation from the light cone, flattening the k-dependence and bringing it closer to the behavior of the cavity resonance (the last partition of Fig.8 with c = 0.18 μm and h = 0.3 μm).

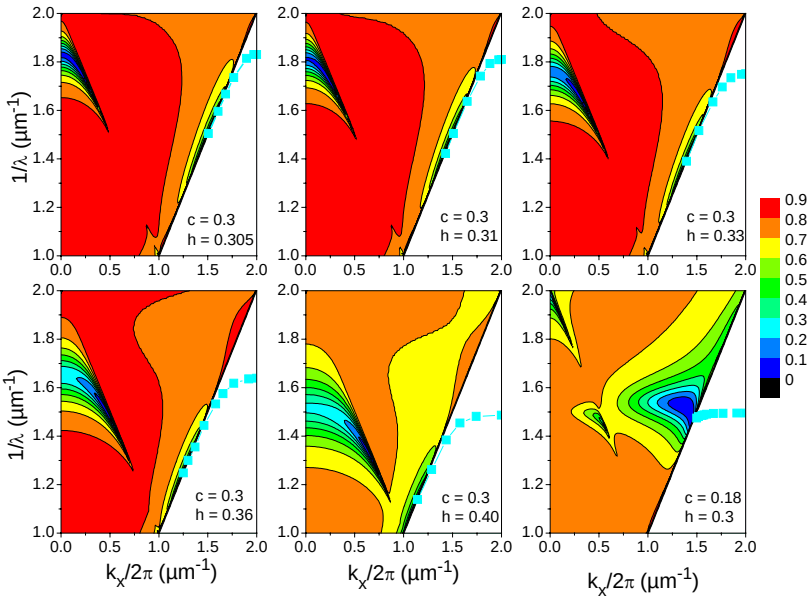

Fig.8. The same as in Fig.7 but with deep grooves for several values of the groove depth and width. The last partition corresponds to a cavity resonance.

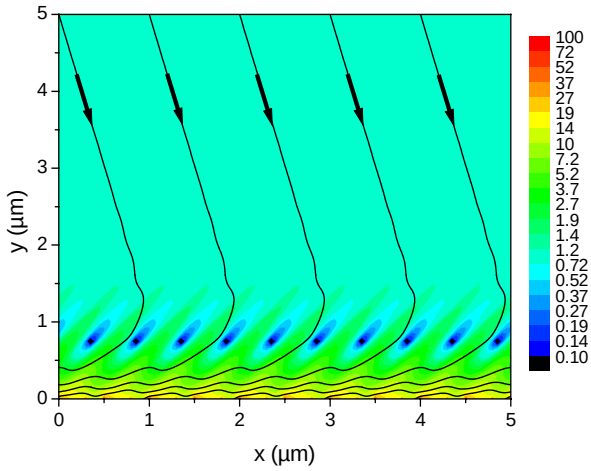

Fig.9. Poynting vector map close to the grating surface, corresponding to the first kind PSW, existing for shallow grooves with parameters corresponding to a total absorption of incident light (c = 0.3 μm, h = 0.036 μm, α = 0.24591). Poynting vector modulus represented by the color pallet and its direction by the black lines.

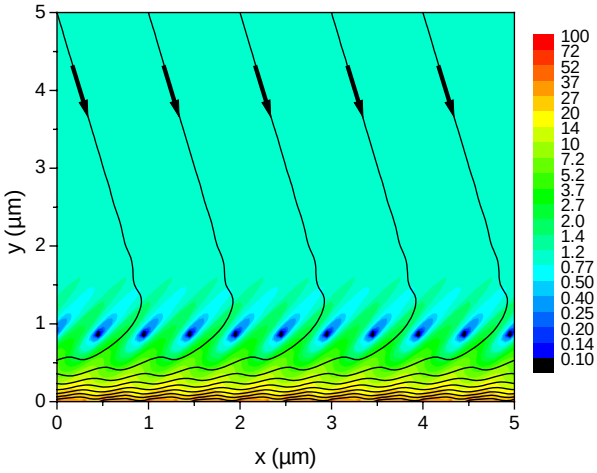

Fig.10. Same as in Fig. 9 but for the second kind of PSW existing for deep grooves with c = 0.3 μm, h = 0.34 μm , α = 0.24705, corresponding to the total absorption of incident light.

The similarity between the dispersion curves of the PSW for shallow and deep grooves can be further stressed when looking at the map of Poynting vector near the grating surface (Fig. 9 for shallow grooves and Fig. 10 for deep grooves). The values of the Poynting vector are normalized so that its modulus for the incident wave is equal to unity. The groove parameters are chosen in such a way that the incident light is fully absorbed due to the resonances. Several wavelengths far from the grating surface, the Poynting vector corresponds to the incident plane wave (no energy in the reflected wave). When approaching the grating surface, the Poynting vector turns almost parallel to the surface, corresponding to a surface wave traveling in –x direction, both for shallow and deep grooves, pointing to the common nature of the two kinds of resonances.

Moreover, in the two cases there is a significant increase in the energy density close to the grating surface (by almost two orders of magnitude), a typical feature of the surface wave excitation, contrary to the cavity resonances [9], although it is possible to obtain an almost

total absorption of incident light when cavity resonances are excited. For example, for groove dimensions c = 0.195 μm and h = 0.306 μm, the total reflected energy becomes less that 7% at incidence α = 0.92389 (order 0 carries about 2.5% and order –1 the rest). However, despite the high absorption, the behavior of the near-field is completely different, as observed in Fig. 11. Neither the Poynting vector represents a surface wave close to the surface, nor there is a significant increase in the local energy density. The weak fluctuations of the direction and modulus of the Poynting vector observed in the near and far-field regions are due to the interference between the incident and the reflected waves.

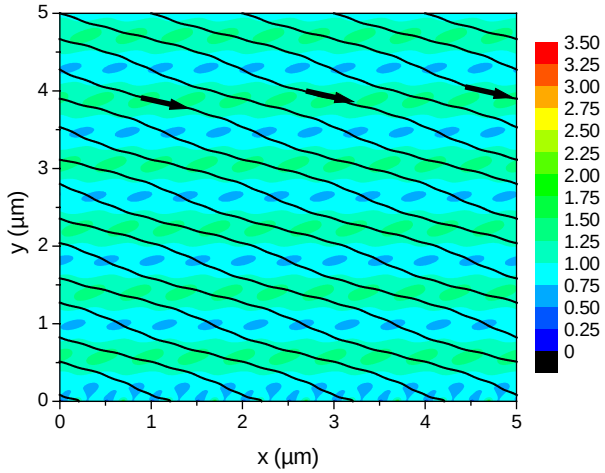

Fig.11. Same as in Fig. 9 but for the cavity resonance with groove parameters corresponding to high absorption of incident light, c = 0.195 μm, h = 0.306 μm, and α = 0.92389.

In order to explain the differences between the first and the second kind of PSW it is necessary to look inside the groove by calculating the electric field and the Poynting vector defined as the half of the real part of the vector product ofthe electric field and the complex conjugate magnetic field: $\mathbf{P} = \mathrm{Re}(\mathbf{E} \times \bar{\mathbf{H}})/2$. For shallow gratings, the electric field distribution and the Poynting vector behavior inside the shallow groove are almost the same on the top of the lamella as at the groove bottom, as observed in Fig.12(a) and in Fig.13(a), leading to approximately the same absorption through the lamellae top and the grooves bottoms. On the contrary, the deep groove modifies significantly the field behavior. The appearance of the second kind of PSW requires a resonance of the electric field inside the grooves, as already shown in [10]. As observed in Fig.12(b), the Poynting vector on the lamella top and groove opening forms a continuous flow, quite similar to the picture in shallow gratings. Due to the high conductivity of aluminum in the visible, the tangential component of the electric field almost vanishes on the metallic surface. As a consequence, the x-component of the electric field has a minimum at the groove bottom, as well as at the lamella top (see Fig.13(b)). Its value on the groove opening (y = h) depends on the groove depth and the wavelength. When the groove depth is close to a half-wavelength value, inside the groove there appears a standing wave of the fundamental (TEM) mode that can be supported by the hollow metallic waveguide formed between the groove sidewalls. In that case, there is a minimum of $|E_x|$ at the groove opening, and thus the boundary conditions over the entire plane y = h over the grooves and lamellae are almost identical to the conditions on a flat metallic surface. As far as the latter can support PSW, the similarity in the boundary conditions at y = h for deep grooves leads to appearance of the second kind of PSW. As observed in Fig. 5, this PSW can have losses smaller than the plasmon on a flat surface, if the real part of its propagating constant is close to k_0. The explanation can be found in the fact

that when $\alpha \approx 1$, the PSW extends a lot inside the covering dielectric and its energy is less localized in the metal.

The field map peculiarities of this second kind PSW as given in Fig.13(b) can explain the behavior of the dispersion curves in Fig. 8. In particular, one observes that at a given value of groove parameters (width and depth), there exist a cut-off frequency for the second kind of PSW, below which the effective refractive index crosses the light cone and the wave is radiated into the cladding. This can be explained by the fact that for lower frequencies (i.e., longer wavelengths), the grooves must be deeper in order that a half-wavelength resonance of E_x fits inside it (otherwise the absorption is so strong that the plasmon surface wave cannot propagate). This is the reason why the cut-off frequency is reduced when the groove depth is increased in Fig. 8, deeper grooves can better support longer wavelength. One can observe also at y=-0.2 μm a semi-curl of the energy flow inside the groove, similar to the complete curl observed already in [22]. The difference lies in the groove width which is in our case too small to allow an entire swirl of the energy flow.

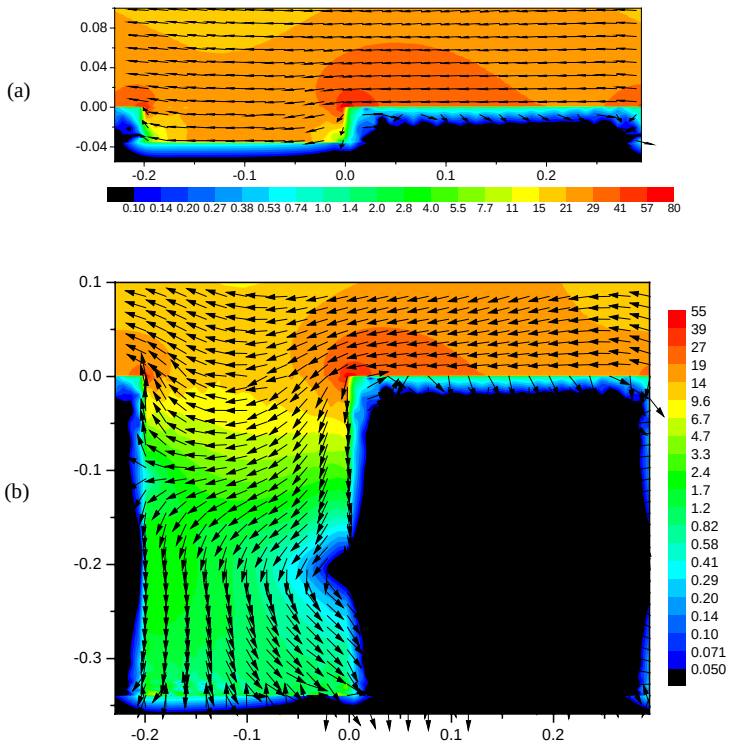

Fig.12. Poynting vector maps inside the shallow (a) and deep (b) grooves corresponding to the first and the second kind of PSW.

As can be expected, when the groove depth is doubled, the standing wave of the TEM mode inside the groove leads to another resonance, similar to the case presented in Fig. 13(b). A third branch of PSW appears at groove depth values, for which the x-component of the electric field almost vanishes at the groove opening, as shown in Fig. 14(a). This new branch can also be accompanied by a total absorption of the incident light, Fig. 14(b).

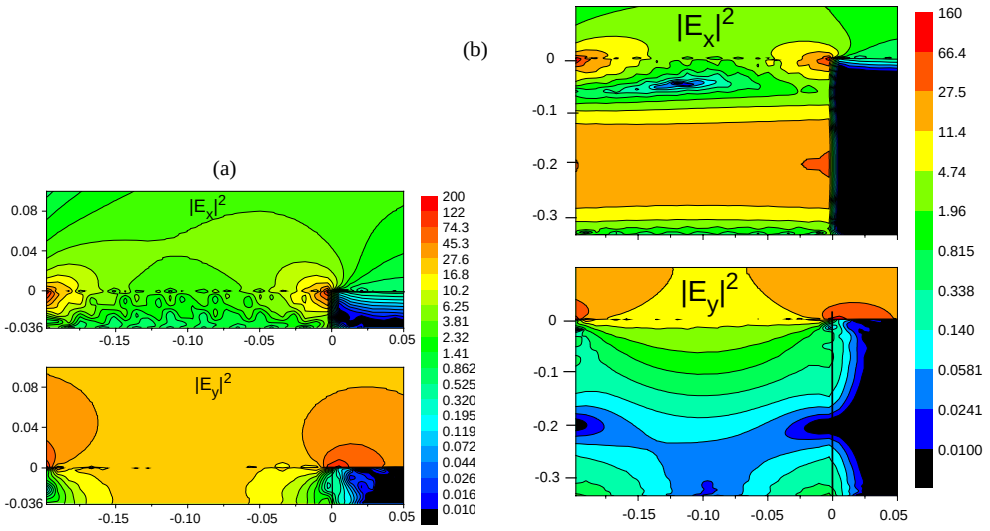

Fig.13. x- and y-components of the electric field normalized with respect to the incident wave amplitude for shallow (a) and deep (b) grooves.

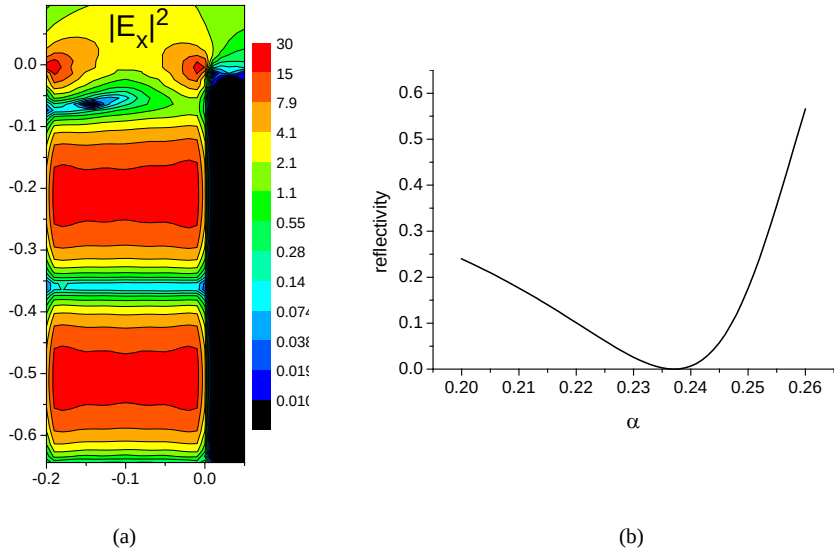

Fig.14. The map of the x-component of the electric field inside the groove of a deep lamellar grating (a) with h = 0.644 μm, accompanied by a total absorption of the incident light, as observed in the angular dependence (b).

A natural question that arises from the comparison between shallow and deep gratings, is whether the PSW in deep gratings behaves like a surface wave when its dispersion curve moves away from the light cone with the decrease of the wavelength values, observed in Fig. 8. This question becomes even more important, because in this region the dispersion curve of the PSW starts to behave like a cavity resonance, as observed in the last partition of Fig. 8. Fig. 15 presents the Poynting vector map above the grooves of a grating with h = 0.40 μm, c = 0.30 μm (presented in the middle of the lower line in Fig. 8) and with a working point corresponding to the flat region of the dispersion curve with $k_x / 2\pi = 1.74\,\mu m^{-1}$ and $1/\lambda$ = 1.5. As can be observed, contrary to Fig. 11, close to the grating surface the vector turns in

direction corresponding to a surface wave excitation through order –1, and there is an increase in its density, although smaller than in Figs.9 and 10.

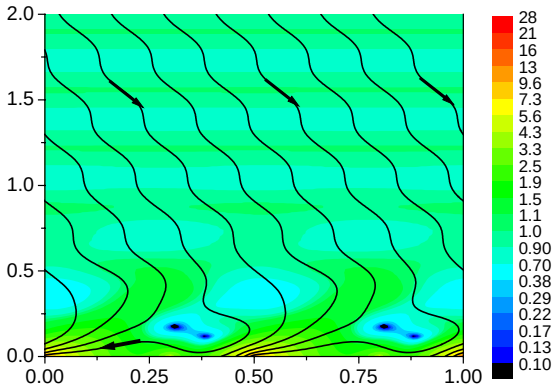

Fig.15. Poynting vector modulus (color pallet) and its vector lines for a grating with h = 0.4, c = 0.3 μm, $\lambda = 0.675$ μm and $\alpha = 0.258$.

Another interesting feature observed in Fig. 8 is the existence of a second region of high absorption situated in grazing incidence just in the vicinity of the light cone. Its appearance is even more surprising when one takes in fact that at these angles of incidence the grating can support two propagating diffraction orders, so that high absorption requires that their efficiencies are simultaneously suppressed. And indeed, this is the case as shown in Fig. 16. The groove parameters for this value of the wavelength correspond to the region just below the cut-off, as in the figure the groove depth h = 0.294 μm, while the plasmon propagation constant starts to be greater than k_0 for h > 0.304 μm). It is well-known than when the trajectory of the mode propagation constant crosses the cut-off, the pole corresponding to the modal resonance is transformed into a zero of the zeroth diffracted order [23], responsible for the minimum of the diffraction efficiency in this order, observed in Fig. 15. On the other hand, the curl of the Poynting vector which fills almost entirely inside the groove separates the groove bottom from the incident wave and decreases the diffraction in order –1, thus its efficiency remains low in a large interval of angles of incidence.

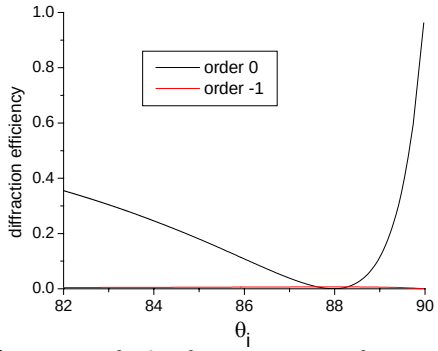

Fig.16. Diffraction efficiency in order 0 and –1 in grazing incidence. Wavelength 0.6328 μm, groove width c = 0.3 μm, and groove depth h = 0.294 μm.

4. Two-dimensional (crossed) gratings

When considering the extension of the preceding results to biperiodic grating, two straightforward possibilities can be envisaged. The first one is to consider a grating consisting in a biperiodic layout of metallic blocks that can also bee seen as crossed slits (Fig. 1b). There are few and obvious differences between this configuration and the one-dimensional grating we have studied above. We have numerically checked that for similar parameters the same effects can be observed. Further details on such structures can be found in a recent article by A.-L. Baudrion et. al (see for example Fig. 10 of [24]).

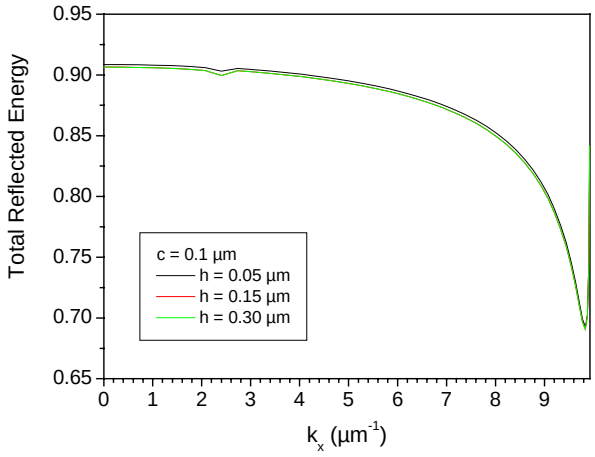

Fig. 17. Total reflected energy by a periodic array (d = 0.5 μm) of square finite-depth holes in an aluminum substrate with side-wall length c = 0.1 μm. Wavelength of 0.6328 μm, incident magnetic field vector parallel to the metallic surface, and the plane of incidence parallel to the hole walls.

The second possible geometry consists in a bi-periodic array of holes. In this case one notable difference is the existence of a cut-off for the propagating modes inside the holes [7-8,25], when considering them as metallic waveguides. For square holes (or any simply-connected cross section), the fundamental TEM modes has a cut-of frequency, which does not exist for slits. And indeed, as in the case of the so-called extraordinary transmission, one can expect that the slits and hole will have very different behaviour. In order to emphasize this difference we show in Fig. 17 the total reflected energy for three values of the square hole's edges *c*. As previously, we consider gratings made of aluminium with a period of d = 0.5 μm and a wavelength λ = 0.6328 μm. The incident plane wave is assumed to be polarized so that the electric field vector lies in the incident wave-vector plane (i.e. the magnetic field is parallel to the grating plane). For a small value of c (*c* = 0.1 μm), Fig. 17 shows that the hole depth h doesn't have a significant influence on the reflectivity of the structure, the total reflected energy curves are hardly distinguishable for h = 0.05 μm to 0.3 μm. For c = 0.3 μm and c = 0.4 μm, the behaviour is different and one can easily see that the depth of the hole strongly influences the reflection. This can be easily understood by taking into account the fact that for c = 0.1 μm, contrarily to the two other cases, no propagating modes exist in the holes. Thus, due to the exponential decay of the non-propagating modes, the electromagnetic field barely reaches the bottom of the holes and it is not surprising that the depth of the holes is of little importance. A comparison between c = 0.3 and 0.4 μm in Figs. 18-19 shows first that almost total absorption can be obtained for c = 0.3 μm with a relatively low sensitivity to the depth of the hole, while for c = 0.4 μm, the behaviour seems to be much more sensitive to h. Here again the understanding comes from the behaviour of the modes in the holes, as λ = 0.6328 μm is close to the cut-off wavelength for c = 0.3 μm thus in that case the absorption (as well as nonlinear effects [26]) can be enhanced significantly [27]. For c = 0.4 μm, the

oscillation of the amplitude of the absorption peaks can be understood as the consequence of the Fabry-Perot modes in the holes.

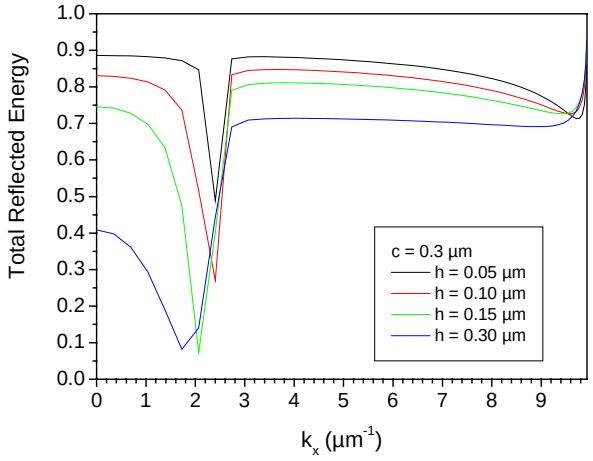

Fig. 18. Same as in Fig. 17, but for larger holes with side wall length c = 0.3 µm.

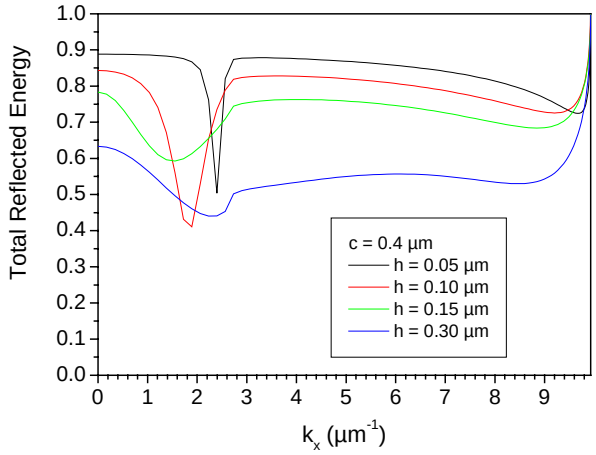

Fig. 19. Same as in Figs. 17 and 18, but for c = 0.4 µm.

The support of EC-funded project PHOREMOST (FP6/2003/IST/2-511616) is gratefully acknowledged.